First International Conference on Damage Tolerance of Aircraft Structures
R. Benedictus, J. Schijve, R.C. Alderliesten, J.J. Homan (Eds.)

RESIDUAL STRENGTH PREDICTION OF A STIFFENED PANEL USING THE COHESIVE MODEL

Ingo Scheider*

*GKSS Research Centre, Institute of Materials Research
Max-Planck-Str. 1, 21502 Geesthacht, Germany
e-mail: ingo.scheider@gkss.de
Web page: www.gkss.de

Abstract. *The residual strength of a flat aluminium panel with five stringers, which contained a crack that divided the central stringer, was to be predicted during a Round Robin organised by ASTM. Crack branching occurred in the experiment, when the crack extended along the skin and into the stringers. The prediction has been achieved using finite element simulations including a cohesive model for crack extension. In a first step, the crack extension parameters, cohesive strength, T_0, and cohesive energy, Γ_0, were determined by numerical reproduction of the experimental data of the M(T) specimen. With the optimised parameters, the five-stringer panel was modelled. It turned out that the deviation of the predicted residual strength from the experimental value was below 9%. It will also be shown that shell elements cannot be used for this kind of simulation due to the high constraint in front of the crack tip, which leads to plastic collapse if plane stress conditions are presumed.*

1 INTRODUCTION

Advanced methods for the prediction of residual strength and thus structural fracture assessment are often based on numerical approaches and use models for crack extension embedded in the simulation of the real component. One model that has gained increasing attraction is the cohesive model, which is based on an idea proposed by Dugdale [1] and Barenblatt [2] also in the early 60's. The first one, who used the cohesive model in combination with the finite element method for the simulation of ductile failure in metals, was Needleman in 1987 [3]. The application to the assessment of metallic structures has been focused in several publications, see e.g. [4], [5].

Naturally, due to computational limitations, the cohesive model has been used for two-dimensional simulations first, but in the late 90's, when computers became more powerful, 3D simulations were performed as well [6] - [9], which gave a more realistic approximation of the processes ahead of the crack tip. For example, the numerical reproduction of crack front tunnelling as shown in [9], is only possible by a 3D analysis.

Thin-walled structures are also a point of interest for a couple of years, and so cohesive elements have been developed for plane stress and shell elements. The problem with these types of structures is that the thickness change cannot directly be accounted for in the cohesive elements, since the interface only consists of a line, which by definition has no thickness. Therefore, cohesive elements have been developed that were able to take the actual thickness of the adjacent plane stress or shell elements into account, see e.g. [10]- [13].

Even though the cohesive model is in a state, in which it can be applied to complex

engineering structures, this application field has gained only very little attention, see e.g. **[14]**. Therefore, the current investigation is aimed at demonstrating the applicability to components, for which the standard procedures cannot be applied with sufficient accuracy.

The structure under investigation is a five-stringer panel, which is part of an ongoing Round Robin organised by ASTM. During the first phase of the Round Robin, three different panels machined from a monolithic Al 2024-T361 block, had to be analysed with respect to fatigue crack growth, but only one of them, shown in Figure 1, was tested for residual strength afterwards.

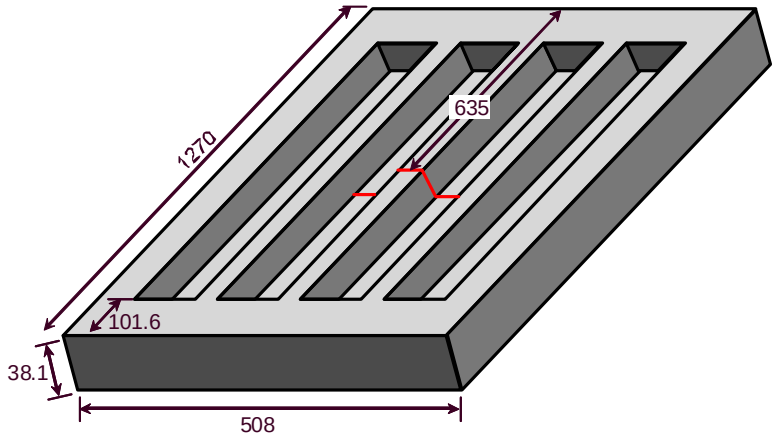

Figure 1: Five-stringer panel containing a crack that divides the central stringer. All dimensions in mm.

For the elastic-plastic properties of the panel, only three distinct values were provided, namely the yield strength, $\sigma_Y = 342$ MPa, the ultimate tensile strength, $R_m = 485$ MPa, and the elongation at ultimate strength, A = 18.3 %, were given for the material. The stress-strain curve is generated out of these values by the following procedure: The engineering values first were converted in true-stress – log-strain values, and then a power-law fit of the form $\sigma_Y = \sigma_{Y,0}\left(\varepsilon/\varepsilon_Y\right)^n$ with $\sigma_{Y,0} = 342$ MPa, $\varepsilon_Y = 0.00503$ and $n = 0.14745$ was employed to connect the yield and the ultimate tensile point. This constructed curve was then used for all subsequent simulations.

The fracture properties of the material were given data determined by a test on an M(T) panel with a width of $2W = 400$ mm, a thickness $t = 6.44$ mm and an initial crack length of $2a_0 = 103$ mm. From this test three different values are measured: the force, F, the crack mouth opening displacement, COD, and the crack extension, Δa. Based on these data, the F(COD) curve and a COD(Δa) curve are used for numerical identification.

2 NUMERICAL MODEL

As outlined already, the cohesive model is utilised for the numerical crack extension analyses. It is implemented as a user-defined interface element for arbitrary material decohesion processes within the finite element code ABAQUS and obeys a so-called traction-

separation law (TSL) as a constitutive behaviour, which relates the displacement jump vector between the two sides of the interface, $\boldsymbol{\delta}$, to the traction vector, $\mathbf{T}(\boldsymbol{\delta})$, acting on the interface. In many cases the one-dimensional representation of the relation is sufficient, namely when only mode I fracture is concerned. The constitutive behaviour can then be written in the form $T_N = f(\delta_N)$, in which the subscript N denotes the normal component of the separation and traction, respectively (and will be omitted further on). Many different laws have been used in the literature, see e.g. the overview given in **[16]**. The effect of the shape on the crack extension results are discussed e.g. in **[17]**. In the present investigation the function f is described by the following equation **[15]**:

$$T = T_0 f(\delta) = T_0 \begin{cases} 2\left(\frac{\delta}{\delta_1}\right) - \left(\frac{\delta}{\delta_1}\right)^2 & \delta < \delta_1 \\ 1 & \delta_1 < \delta < \delta_2 \\ 2\left(\frac{\delta - \delta_2}{\delta_0 - \delta_2}\right)^3 - 3\left(\frac{\delta - \delta_2}{\delta_0 - \delta_2}\right)^2 + 1 & \delta_2 < \delta < \delta_0 \end{cases} \tag{1}$$

with $\delta_1 = 0.01\ \delta_0$, and $\delta_2 = 0.75\ \delta_0$ in all simulations.

The interface elements are available for 2D, shell and 3D finite element models. Since the structure under investigation is a complex thin-walled one, the only choice is between shell and 3D modelling. The cohesive elements for shells are of line shape, such that the upper and the lower lines are defined by two nodes each. In the undeformed state these lines are on top of each other, i.e. they do not span a finite area. As already pointed out, the cohesive shell interface cannot account for a thickness change by default. However, the current implementation allows for transferring the out-of-plane deformation of the adjacent shell element to the cohesive element by internal variables via user programming, see **[11]**. For three-dimensional structures, the interface is defined by 2D elements with 8 nodes, which again do not span a volume in the undeformed state.

3 FINITE ELEMENT MODELLING

Structures, which might be regarded as thin walled, are commonly modelled by shell elements in industrial applications due to cost and time saving requirements. Therefore the use of shell elements is favoured in the present case.

The task is to predict the mechanical behaviour of the five-stringer panel by numerical simulations. In order to do so, the parameters for the cohesive model have to be identified first, which will be performed by reproducing the experimental F(COD) curve and the COD(Δa) curve of the M(T) specimen. This two-parameter fitting process much depends on experience, and no optimisation procedure has been employed, but the adjustment is performed by trial and error only.

3.1 Parameter identification

One quarter of the M(T) specimen is to be modelled due to symmetry. A line of cohesive elements is placed along the ligament consisting of 160 cohesive elements with a length of

0.25 mm, thus allowing for 40 mm crack extension. The mesh consists of 2903 linear shell elements, and the total number of degrees of freedom is 18789.

Force, COD and crack extension are evaluated and the optimal parameters are identified based on the COD(Δa) curve, leading to $\Gamma_0 = 13$ kJ/m² and $T_0 = 730$ MPa. With these values, the critical separation writes $\delta_0 = 0.020$ mm.

The corresponding curves from the simulation with these parameters are shown in Figure 2 indicating a very good agreement between experiment and simulation.

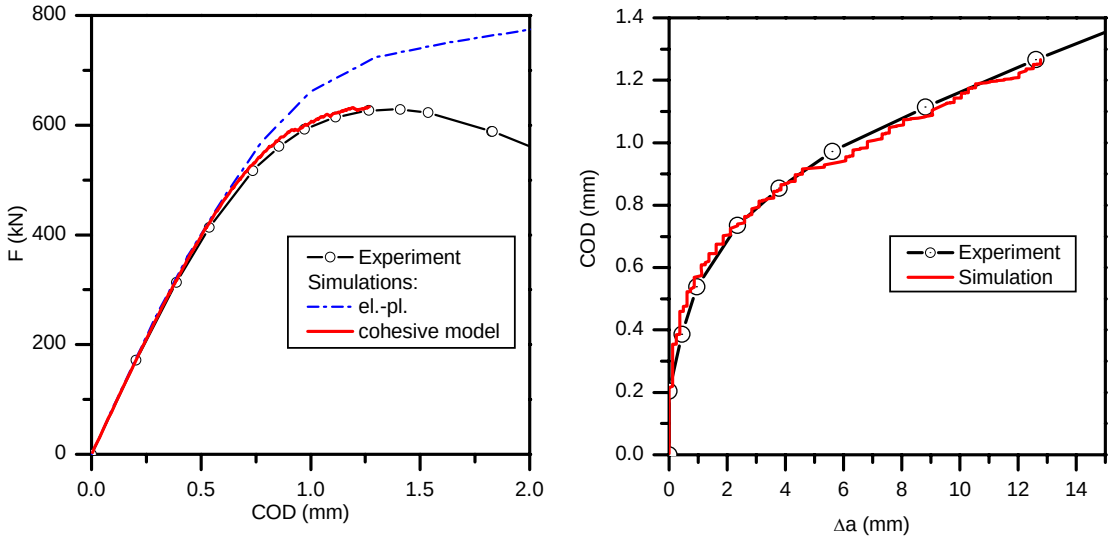

Figure 2: Comparison between experiment of the M(T) specimen and simulation with optimized parameters; a) F(COD) curve; b) COD(Δa) curve.

3.2 Application to the stiffened structure

The parameter identification revealed that both the global F(COD) curve and the COD(Δa) curve can be reproduced and thus the use of shell modelling seems to be possible, and a shell mesh is generated for the five-stringer panel of Figure 1. Due to symmetry only one quarter of the structure is to be modelled. The clamping region at the top of the structure is assumed to have little effect on the result of the simulation and is therefore not modelled. A vertical displacement is prescribed, instead, where this region begins. The quantities that are evaluated from the simulation are: force, *F,* crack extension, *Δa*, and crack opening displacement (COD) as shown in Figure 3

The experimental σ_{appl}(COD) curve with $\sigma_{appl} = F/A$ being the applied stress ($A = 5110$ mm² is the cross section of the uncracked structure), have been provided by ASTM after completion of the round robin for comparison with the numerical results.

Shortly after initiation, the crack branches into skin and stringer; therefore cohesive elements must be placed along both lines. Since it is not known how much crack extension can be expected before maximum load, the cohesive elements were placed in the whole stringer and 40 mm along the skin. With a cohesive element length of approx. 0.25 mm this

leads to 161 elements along the skin and 102 elements at the stringer. The number of shell elements in the model is 8782, which gives 56070 DOFs in total.

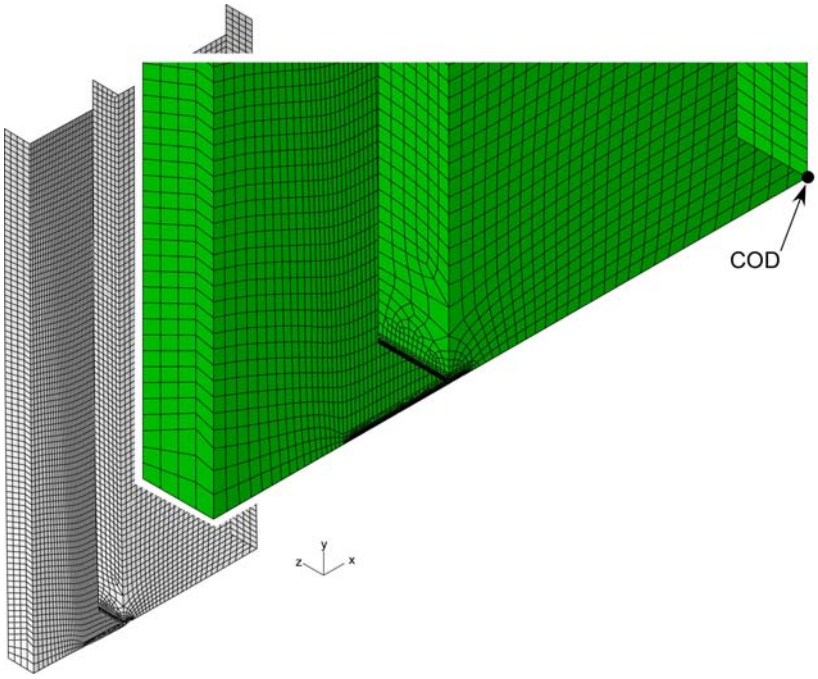

Figure 3: Shell finite element mesh for the five-stringer panel (one quarter of the original structure due to symmetry).

Though the same parameters and a similar finite element mesh size are used as for the M(T) panel, the simulation reveals that a realistic prediction of the structural response is not possible with the shell model. As shown in Figure 4, strain localisation occurs in the shell elements adjacent to the cohesive surface, which leads to local softening instead of crack extension. The reason for this behaviour is that high normal stresses in crack opening direction together with low triaxiality due to the plane stress assumption lead to high plastic straining and subsequent plastic collapse of the elements ahead of the crack tip. In reality, however, plasticity is reduced by the high constraint at the crack tip. Therefore, even though the structure may be regarded as thin walled by the geometrical and structural definition given in the introduction, it cannot be modelled by shell elements due to the violation of the mechanical plane stress condition in the crack tip region

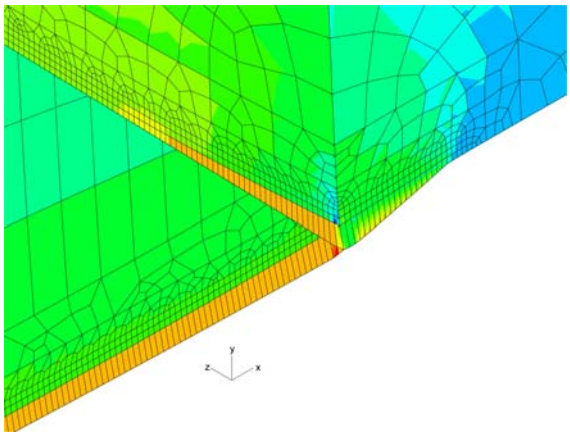

Figure 4: Pathological deformation in the shell elements adjacent to the cohesive layer due to stress localization and softening, which inhibits crack extension.

4 3D FINITE ELEMENT MODELLING

The previous section showed that it is not possible to model the five-stringer panel with shell elements. The only possibility to take the stress state at the crack tip into account is to model the structure with 3D continuum elements, even though this means a vast increase in the model size and thus computation time. A small reduction of the problem may be achieved by coupling a 3D mesh for the crack tip region to a shell mesh for the global structure, but since approximately 90% of all elements are placed along the ligament, the savings are not worth the additional meshing effort.

According to the results achieved by Zavattieri **[13]**, which correspond to the authors' experience, the parameters determined by a 3D simulation are different from those determined by a shell simulation. Therefore, if the prediction is performed with a specific element type, the same type has to be used for the parameter identification of the material.

The 3D FE model of the M(T) specimen represents one eighth of the panel with three symmetry planes and consists of 30408 linear 3D elements. 15 layers of solid elements over the half thickness are generated in the ligament, varying between a width of 0.45 mm in the centre and 0.075 mm at the specimen surface, and their length being 0.15 mm. The cohesive surface consists of $15 \times 200 = 3000$ cohesive elements, thus allowing for a maximum crack extension of 30 mm. The whole model has 113472 degrees of freedom.

The loading is applied by a prescribed displacement at the top of the specimen. As a result, the total force, F, COD and the crack extension, Δa, (averaged over the thickness) is determined. The comparisons between simulation and experiment with respect to the F(COD) and COD(Δa) curves are shown in Figure 5. The optimal parameter set for the 3D simulation is $\Gamma_0 = 20$ MPa and $T_0 = 970$ MPa, the critical separation resulting in $\delta_0 = 0.024$ mm. Both the cohesive strength and the cohesive energy are larger than those for the shell simulation. At least for the cohesive strength, this phenomenon has been reported already by Zavattieri **[13]**

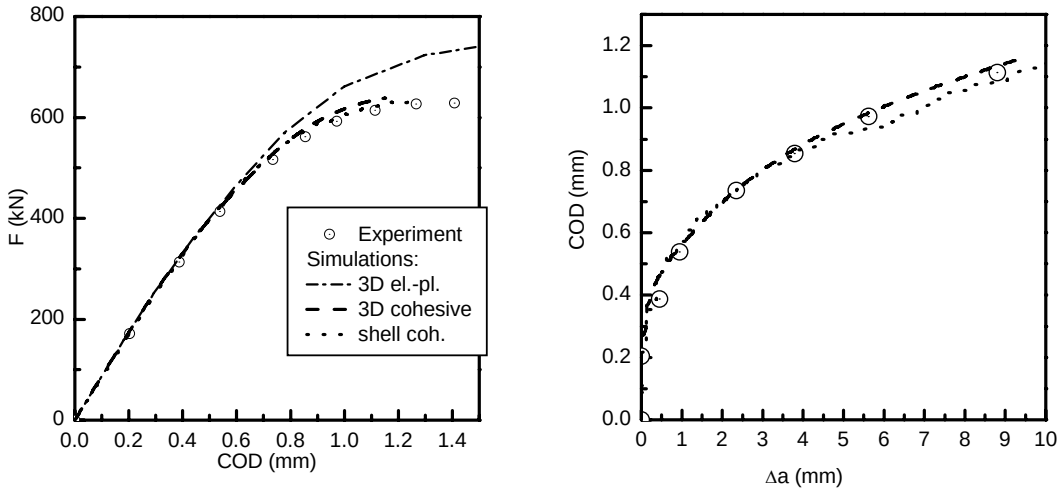

Figure 5: Parameter identification for the 3D FE model of the M(T) specimen. Comparison of simulation and experiment for the respective optimised parameter sets.

Due to the large computation time, the simulation was stopped after approximately 9 mm of crack extension. At this time, the force was very close to the residual strength of the specimen. Additionally, the results of an elastic-plastic simulation (without crack propagation) are shown in the F(COD) graph. From this curve, the effect of crack propagation becomes evident.

The stress state in front of the crack tip is commonly characterised by the triaxiality $h = \frac{1}{3}\sigma_{kk}/\sigma_{eq}$, which is shown in Figure 6 at the time of crack initiation (left) and at the end of the simulation (right). One can see that the maximum triaxiality is higher at initiation than at the end of the simulation, but the region of triaxiality $h > 2/3$ (bordered by black lines) increases during crack extension. For a structure under plane stress condition, i.e. the out-of-plane stress component being zero, the triaxiality cannot exceed $h = 2/3$. It is obvious that the actual stress state with a triaxiality up to $h = 1.5$ cannot be characterised locally as plane stress. Even though it was possible to reproduce the results of the M(T) specimen with shell elements (see above), the transferability of the parameters is highly questionable, if the high triaxiality is not taken into account.

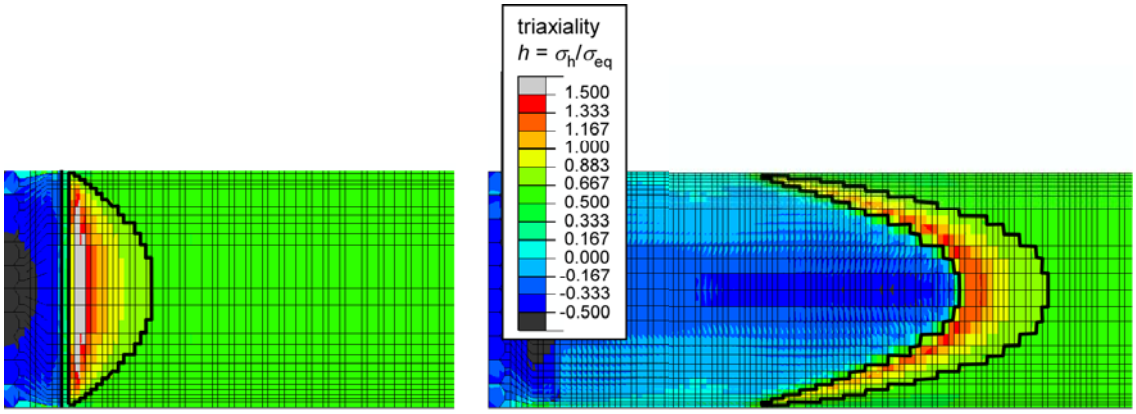

Figure 6: Local triaxiality of the M(T) specimen ahead of the crack tip. Left: at crack initiation; right: at end of simulation. The thicker black polygon indicates the region in which the triaxiality is higher than 2/3.

For the second step, the simulation of the stiffened panel, a 3D finite element model containing one quarter of the whole structure, shown in Figure 7, has been generated. The same region as for the shell mesh has been supplied with cohesive elements, but now 15 elements over the stringer thickness and 24 over the skin thickness are introduced, which leads to 4625 cohesive elements in total with a size of approx. 0.3×0.3 mm² each. The whole structure contains 41294 3D elements and has 170397 DOFs.

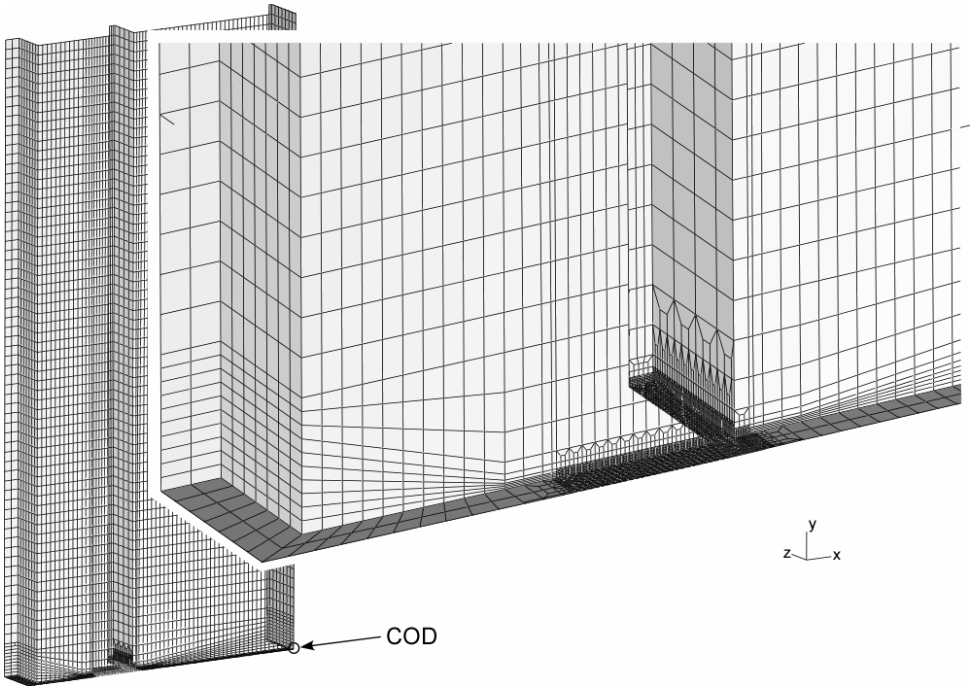

Figure 7: 3D finite element mesh for the five-stringer panel (one quarter due to symmetry).

The comparison of the simulation with the experiment is shown in Figure 8. The residual strength in the simulation is 135 MPa compared to 148 MPa in the experiment, which is a deviation of less than 9%. It is worth noting that the prediction is conservative in the present case, which is an important point in structural assessment. However, it is not assured in general that the method will always yield conservative results.

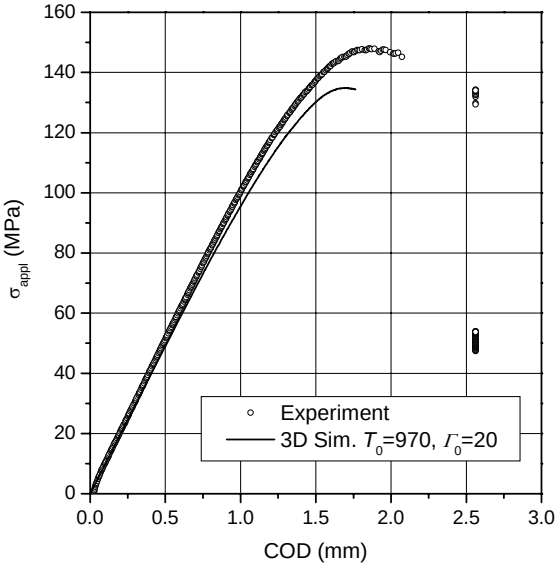

Figure 8: Comparison of the global applied stress vs. COD curves between experiment and 3D simulation.

6 CONCLUSION

It has been shown that the cohesive model is able to predict crack extension and residual strength of complex structures. The approach follows a two-step procedure: First the cohesive parameters have been determined by simulation of an M(T) specimen and fitting of the numerical results to the experiment, and subsequently a five-stringer panel has been simulated with the optimised parameter set. The results show that the parameters can be transferred from

fracture mechanics specimens to structures and yield realistic predictions.

The residual strength has been predicted by three participants in a Round Robin organised by ASTM. Two used a *J*-integral approach for the assessment, but the cohesive-model simulation presented here was closest to the experimental result; the maximum stress in the simulation was 135 MPa (compared to 148 MPa in the experiment), whereas the other two participants predicted 129 MPa and 120 MPa, respectively.

The predictions based on conventional fracture mechanics parameters as J or K_{eff} face several problems: Firstly, J as a path integral cannot be calculated when structural or material inhomogeneities are present close to the crack tip, which is the case here due to the stringer connection. Likewise the stress intensity factor cannot be calculated since there is no valid K field in the neighbourhood of the stringer connection. In addition, no analytical solutions exist for fracture mechanics parameters in stiffened panels, if the crack approaches the joint.

The cohesive model is able to describe any kind of material separation, even without a pre-existing crack, and therefore no restrictions exist due to non-existing or non-valid fracture parameters. Thus, the main advantage is not mainly a higher accuracy compared to conventional fracture mechanics analyses, but the ability to predict complex geometries and crack shapes. Another argument in favour of this model is that local variation of the material properties as weldments with changed yielding behaviour or residual stresses can be considered in a simple way within the numerical analysis and simultaneously a stress analysis of the structure is delivered, which was used in the present case to determine the stress triaxiality in the crack tip region, for example.

One important point is the applicability of shell meshes to thin walled structures containing cracks. Even though the global behaviour of the present structure is mainly plane stress, it has been shown that the stress state in front of the crack tip contains a region with a triaxiality higher than $\sigma_h/\sigma_{eq} = 1.5$. Since such high triaxialities cannot be accounted for by a shell theory, shell elements must not be used. In the present case the shell simulation of the stiffened panel with cohesive parameters determined by the M(T) specimen did not lead to crack extension, but to plastic collapse of the shell elements adjacent to the ligament. However, for 3 mm thick aluminium material, transferability has been shown from C(T) specimens to M(T) and cruciform specimens, see **[12]**.

The 3D simulation was rather costly in terms of meshing and simulation time, indeed, but the good agreement between experiment and simulation justifies the effort. The amount of crack extension before maximum load may be very large especially in thin walled structures, such that many (in the present case more than 4500) cohesive elements had to be inserted into the model, but computer power is steadily increasing and therefore this issue will diminish in the future.

REFERENCES

[1] D. S. Dugdale, “Yielding of steel sheets containing slits”, *J. mech. Phys. Solids* **8**, 100-108 (1960).

[2] G. I. Barenblatt, “The mathematical theory of equilibrium of cracks in brittle fracture”, *Adv. Appl. Mech.* **7**, 55-129 (1962).

[3] Needleman, “A continuum model for void nucleation by inclusion debonding”. *J. Appl. Mech.* **54**, 525-531 (1987).

[4] Cornec, I. Scheider, K.-H. Schwalbe, “On the practical application of the cohesive model”, *Eng. Fract. Mech.* **70**, 1963-1987 (2003).

[5] H. Yuan, G. Lin and A. Cornec, “Verification of a cohesive zone model for ductile fracture”. *J Engng Mater Technol.* **118**, 192–200 (1996).

[6] G. Lin, A. Cornec and K.-H. Schwalbe, “Three-dimensional finite element simulation of crack extension in aluminium alloy 2024-FC”. *Fatigue Fract. Engng. Mat. Struct.* **21**, 1159-1173 (1998).

[7] G. Ruiz, A. Pandolfi and M. Ortiz. “Three-dimensional cohesive modelling of dynamic mixed-mode fracture”. *Int J Numer. Meth. Engng*. **52**, 97–120 (2001).

[8] Y. A. Roy and R. H. Dodds, “Simulation of ductile crack growth in thin aluminium panel using 3-D surface cohesive elements”. *Int. J. Fracture* **111**, 21-45 (2001).

[9] C. R. Chen, O. Kolednik, I. Scheider, T. Siegmund, A. Tatschl and F. D. Fischer, “On the determination of the cohesive zone parameters for the modeling of micro-ductile crack growth in thick specimens”. *Int. J. Fracture* **120**, 517-536 (2003).

[10] W. Li, and T. Siegmund, “An analysis of crack growth in thin-sheet metal via a cohesive zone model”. *Eng. Fract. Mech.* **69**, 2073-2093 (2002).

[11] I. Scheider and W. Brocks, “Cohesive model for thin-walled structures”, *Comp. Mater. Sci.* **37**, 101-109 (2006).

[12] I. Scheider, M. Schödel, W. Brocks and W. Schönfeld, “Crack propagation analyses with CTOA and cohesive model: Comparison and experimental validation”, *Eng. Fract. Mech.* **73**, 252-263 (2006).

[13] P. Zavattieri, ^”Modeling of crack propagation in thin-walled structures”, *Trans. ASME, J. Appl. Mech.* **73**, 948-958 (2006).

[14] I. Scheider and S. Heartness, “Restfestigkeitsanalyse einer Flugzeugrumpfschale mit Hilfe von benutzerdefinierten Kohäsivelementen”, *Proc. of the 19. German ABAQUS Users' Conference*, Erfurt, Germany, (2006).

[15] I. Scheider and W. Brocks, “Simulation of cup-cone fracture using the cohesive model”, *Eng. Fract. Mech.* **70**, 1943-1961 (2003).

[16] W. Brocks, A. Cornec and I. Scheider, “Computational aspects of nonlinear fracture mechanics”. In: I. Milne, R.O. Ritchie, B. Karihaloo (eds): *Comprehensive Structural Integrity*, Vol. 3, 127-209 (2003).

[17] I. Scheider, and W. Brocks, “The effect of the traction separation law on the results of cohesive zone crack propagation analyses”, *Key Eng. Mater.* **251**, 313-318 (2003).